JARO 14: 863–877 (2013)
DOI: 10.1007/s10162-013-0413-0

JARO
Journal of the Association for Research in Otolaryngology

Research Article

Directional Plasticity Rapidly Improves 3D Vestibulo-Ocular Reflex Alignment in Monkeys Using a Multichannel Vestibular Prosthesis

Chenkai Dai,[1,3] Gene Y. Fridman,[1,3] Bryce Chiang,[1,3] Mehdi A. Rahman,[2,3] Joong Ho Ahn,[1,3] Natan S. Davidovics,[2,3] and Charles C. Della Santina[1,2,3]

[1]*Department of Otolaryngology-Head and Neck Surgery, Johns Hopkins University School of Medicine, Baltimore, USA*

[2]*Biomedical Engineering, Johns Hopkins University School of Medicine, Baltimore, USA*

[3]*Vestibular NeuroEngineering Laboratory, Johns Hopkins School of Medicine, 720 Rutland Ave., Ross Bldg Rm 830, 21205, MD, Baltimore, USA*

Received: 5 September 2012; Accepted: 11 August 2013; Online publication: 8 September 2013

ABSTRACT

Bilateral loss of vestibular sensation can be disabling. We have shown that a multichannel vestibular prosthesis (MVP) can partly restore vestibular sensation as evidenced by improvements in the 3-dimensional angular vestibulo-ocular reflex (3D VOR). However, a key challenge is to minimize misalignment between the axes of eye and head rotation, which is apparently caused by current spread beyond each electrode's targeted nerve branch. We recently reported that rodents wearing a MVP markedly improve 3D VOR alignment during the first week after MVP activation, probably through the same central nervous system adaptive mechanisms that mediate cross-axis adaptation over time in normal individuals wearing prisms that cause visual scene movement about an axis different than the axis of head rotation. We hypothesized that rhesus monkeys would exhibit similar improvements with continuous prosthetic stimulation over time. We created bilateral vestibular deficiency in four rhesus monkeys via intratympanic injection of gentamicin. A MVP was mounted to the cranium, and eye movements in response to whole-body passive rotation in darkness were measured repeatedly over 1 week of continuous head motion-modulated prosthetic electrical stimulation. 3D VOR responses to whole-body rotations about each semicircular canal axis were measured on days 1, 3, and 7 of chronic stimulation. Horizontal VOR gain during 1 Hz, 50 °/s peak whole-body rotations before the prosthesis was turned on was <0.1, which is profoundly below normal (0.94±0.12). On stimulation day 1, VOR gain was 0.4–0.8, but the axis of observed eye movements aligned poorly with head rotation (misalignment range ~30–40 °). Substantial improvement of axis misalignment was observed after 7 days of continuous motion-modulated prosthetic stimulation under normal diurnal lighting. Similar improvements were noted for all animals, all three axes of rotation tested, for all sinusoidal frequencies tested (0.05–5 Hz), and for high-acceleration transient rotations. VOR asymmetry changes did not reach statistical significance, although they did trend toward slight improvement over time. Prior studies had already shown that directional plasticity reduces misalignment when a subject with normal labyrinths views abnormal visual scene movement. Our results show that the converse is also true: individuals receiving misoriented vestibular sensation under normal viewing conditions rapidly

Correspondence to: Chenkai Dai · Vestibular NeuroEngineering Laboratory · Johns Hopkins School of Medicine · 720 Rutland Ave., Ross Bldg Rm 830, 21205, MD, Baltimore, USA. Telephone: +1-410-5028046; fax: +1-410-6142439; email: cdai4@jhmi.edu

adapt to restore a well-aligned 3D VOR. Considering the similarity of VOR physiology across primate species, similar effects are likely to occur in humans using a MVP to treat bilateral vestibular deficiency.

Keywords: vestibular nerve, vestibular prosthesis, vestibular implant, vestibulo-ocular reflex, VOR, labyrinth, bilateral vestibular deficiency, adaptation, electrical stimulation

INTRODUCTION

The vestibular labyrinths provide sensory input to neural circuits that facilitate accurate perception of spatial orientation and heading, support stable posture, and maintain steady vision (reviewed by Carey and Della Santina 2010). Loss of input from both vestibular labyrinths can cause chronic disequilibrium, postural instability, and decreased visual acuity due to illusory movement of the world during head motion (Grunbauer et al. 1998; Minor 1998; Gillespie and Minor 1999). Bilateral loss of vestibular sensation is caused by several ear disorders, including ototoxic drug exposure, ischemia, infection, genetic abnormality, and trauma. Vestibular rehabilitation involving head–eye coordination exercises is the only clinical treatment with demonstrated success in ameliorating deficits due to profound bilateral vestibular deficiency (BVD). Unfortunately, individuals who fail to recover despite rehabilitative therapy currently have no adequate treatment options.

Normally, canal afferents in each of the three mutually orthogonal semicircular canals (SCC) in a vestibular labyrinth are maximally sensitive to head rotation about an axis approximately perpendicular to the mean plane of the corresponding SCC and exhibit a cosine dependence on the angle between the axis of maximal sensitivity (which we hereafter call the SCC axis) and the axis of head rotation (Della Santina et al. 2005a). Thus, each SCC effectively senses one component of 3-dimensional (3D) head angular velocity. Primary afferent fibers in the vestibular nerve's three ampullary nerve branches report head angular velocity to central pathways in the brainstem and cerebellum to control the 3D angular vestibulo-ocular reflex (VOR), which maintains stable vision by driving extraocular muscles to generate eye movements opposite the direction of head rotation. When this reflex fails due to labyrinthine injuries that spare the vestibular nerve, a multichannel vestibular prosthesis (MVP) can help stabilize images on the retinae and normalize perception of head movement by measuring 3D head movement and encoding that movement via electrical stimuli delivered to the ampullary nerves. We previously developed and described such a device, demonstrating its ability to partially restore a normal 3D VOR (Della Santina et al. 2005b, 2010; 2007; Fridman et al. 2010; Davidovics et al. 2011; Dai et al. 2011).

Despite promising results using this approach, current spread or imprecise electrode placement can reduce MVP efficacy through spurious activation of nontarget axons, which manifests as misalignment between the actual and perceived axis of head motion (Della Santina et al. 2007; Fridman et al. 2010; Davidovics et al. 2011; Dai et al. 2011). Reducing this misalignment is a key goal of efforts to translate this technology to clinical application. Improvements in the design of electrode arrays (Hayden et al. 2011), stimulus waveforms (Davidovics et al. 2011), multichannel coding strategies (Fridman et al. 2010), and current steering via multipolar stimulation (Chiang et al. 2011) have all improved misalignment, but some residual current spread and misalignment are unavoidable, so performance will ultimately depend on an implant user's ability to adjust over time to artificial sensory input.

Previous studies showed that the central nervous system can adapt to improve VOR alignment when there is discordance between the head rotation axis encoded by vestibular nerve input and the axis of VOR movements necessary to stabilize images on the retinae. This effect has been examined by rotating a normal subject about one axis while rotating a visual surround about another axis (Schultheis and Robinson 1981; Baker et al. 1986, 1987; Harrison et al. 1986). In those studies, adaptive changes became evident within a few hours of exposure to the altered visual condition and improved but did not completely eliminate VOR misalignment.

Whether the brain can similarly compensate for misalignment due to current spread or suboptimal MVP electrode placement remains an open question with important clinical implications. In previous experiments in chinchillas, we found that adaptive neural mechanisms markedly improve 3D VOR alignment and conjugacy over 1 week of prosthesis use (Dai et al. 2011). We hypothesized that rhesus monkeys, which are very similar to humans in labyrinthine anatomy and VOR physiology, would also exhibit post-activation improvements in 3D VOR gain and alignment.

To test this hypothesis, we measured the time course and ultimate extent of cross-axis adaptation to prosthetically evoked vestibular nerve activity using 3D scleral coil oculography in vestibular-deficient rhesus monkeys. Each monkey was equipped with a head-mounted, continuously active MVP. For 1 week after onset of stimulation, animals underwent periodic examinations of VOR gain and 3D axis during whole-

body passive rotations in darkness about the mean axis of each SCC pair. Considering prior experience with otherwise normal animals adapting to distorted visual input or compensating after unilateral vestibular lesions (Sadeghi et al. 2007; Ushio et al. 2011), we hypothesized that VOR gain for the component about the head rotation axis would remain stable or increase, off-axis components would decline, 3D VOR alignment would improve, and VOR asymmetry (i.e., the normalized difference in VOR gain about a given axis during head toward and away from the implanted labyrinth) would remain stable or improve.

METHODS

Experiment overview

Five adult rhesus monkeys (6–12 kg) were used in this study, which was performed in accordance with a protocol approved by the Johns Hopkins Animal Care and Use Committee, which is accredited by the Association for the Assessment and Accreditation of Laboratory Animal Care International, and consistent with European Community Directive 86/609/EEC. Each monkey was fitted with a plastic head chamber and two scleral coils prior to baseline measurement of VOR responses to passive whole-body rotation in darkness. Four of the monkeys were then implanted with MVP electrode arrays and treated with gentamicin to ablate hair cell mechanosensitivity. VOR responses to whole-body rotation without MVP stimulation were tested 4 weeks after each gentamicin treatment to confirm bilateral loss of vestibular sensation. Six to ten weeks after electrode implantation, the MVP was then mounted to the head (with gyros aligned to SCCs) and activated, and VOR responses to head rotation with motion-modulated prosthetic input were measured for each rhesus monkey on the first (2–4 h after activation), third, and seventh day after the onset of stimulation, with no interim changes in prosthesis settings. In each testing session, eye movements were recorded during sinusoidal head rotations at 0.05, 0.1, 0.2, 0.5, 1, 2, and 5 Hz (peak velocity 50 °/s) about the horizontal (+H, yaw), left anterior/right posterior (+LARP), and right anterior/left posterior (+RALP) SCC axes shown in Figure 1, with the animal always being reoriented as needed to bring the SCC axis of interest coincident with the Earth-vertical axis of a rotating motor. Transient responses to acceleration step (1,000 °/s^2 to 150 °/s peak velocity) whole-body rotations in darkness were also measured. After the prosthesis was powered off on the seventh day, VOR responses to head rotation were measured a final time to confirm the absence of hair cell function. Between VOR test sections, the monkey was released back to home cage

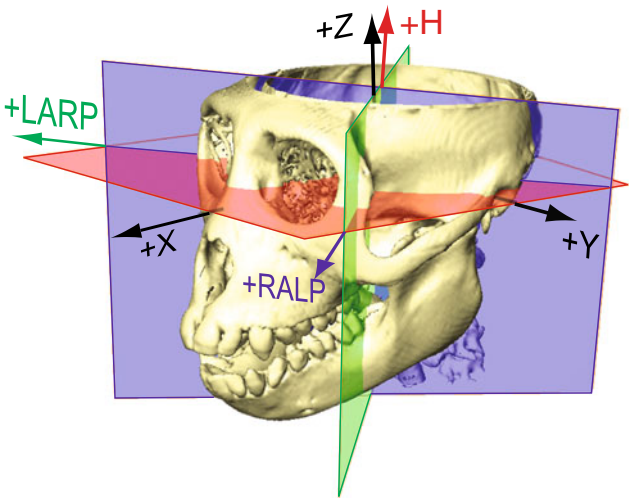

FIG. 1. Semicircular canal (SCC) coordinate system used for the description of head rotation and three-dimensional vestibulo-ocular reflex (3D VOR) eye rotation responses. Skull coordinates +X, +Y, and +Z are mutually orthogonal stereotaxic axes perpendicular to the stereotactic coronal, sagittal, and horizontal planes, respectively. +X is nasal, +Y is out the left ear canal along the interaural axis, the plane containing +X and +Y passes through the inferior-most point of the cephalic edge of each orbital rim, and +Z is superior. SCC coordinate system axes +LARP, +RALP, and +H used in this study approximate the mean SCC axes measured from CT reconstructions of the animals used in this study. They are mutually orthogonal and centered on the XYZ stereotaxic origin. The mean +H axis is close to +Z but pitched back from the stereotaxic +Z axis by 15 ° toward the occiput. The +LARP and +RALP axes are each 45 ° off the midsagittal plane, and 45 ° off the +Y axis, but pitched 15 ° up from the [*X, Y, Z*]=[−1, 1, 0] and [1, 1, 0], respectively. Eye rotation velocity polarities are expressed in this canal-based reference frame using a right-hand rule convention, so that positive eye rotations about +LARP pitch the eye upward while rolling it clockwise (as viewed from behind the head); positive RALP eye rotations pitch the eye downward while rolling it clockwise, and positive H eye rotations yaw the eye to move the pupil toward the left ear.

with visual environment while the prosthesis was continuously modulating. No rewarding was provided for any specific behavior.

Surgical procedures

Details of surgical techniques have been described previously (Chiang et al. 2011; Dai et al. 2011). Briefly, under general anesthesia (isoflurane, 3–5 %), a plastic cylinder-shaped chamber was positioned on the skull in the midline, perpendicular to the mean horizontal SCC plane, to restrain the animal during VOR testing. The axis of this cylinder was pitched 15–18 ° nose-up/top-toward-occiput from the +Z axis perpendicular to the stereotaxic horizontal plane (Fig. 1) as needed to align its axis with the mean axis of the horizontal SCCs measured using multiplanar reconstructions of computed tomography images acquired at 0.5 mm slice thickness using a protocol described in detail previously (Della Santina et al. 2005a) and consistent with prior

published measurements (Black et al. 1996). Two search coils were fashioned from Teflon-coated steel wire (Cooner Wire, Chatsworth, CA) and sutured to the sclera of one globe, with one around the iris and the other approximately orthogonal to the first. Wires were tightly twisted to reduce inductive artifacts and then run to connectors within the head cap.

An electrode array was implanted into the left labyrinth via a transmastoid approach analogous to that used for cochlear implantation. Under sterile conditions, a mastoidectomy was performed. The junction of the ampullae of the superior and horizontal SCCs was identified, and two small holes were made there, keeping a thin strut of bone intact between the two to serve as a stop when inserting a forked electrode array containing a total of six electrodes targeting the ampullary nerves of those SCCs. An opening was also made in the thin segment of the posterior SCC near its junction with the ampulla, into which a second, single-tined array of three electrodes was inserted. Pieces of fascia were tucked around each electrode array, and a small amount of dental cement (Protemp ESPE, 3M Corp.) was used to stabilize the electrode array leads, which were run under periosteum to the head cap.

Eye movement recording and analysis

The eye coil system we use to measure 3D angular eye position has been described in detail previously (Robinson 1963; Migliaccio et al. 2004; Remmel 1984). A monkey was seated in a plastic chair with its head restrained atraumatically by the skull cap, with the head centered within three mutually orthogonal pairs of field-generating coils driven by currents oscillating at 79.4, 52.6, and 40.0 kHz. The cap and restraint imposed a 15–18 ° nose-down pitch of the head's stereotaxic horizontal plane, aligning the mean horizontal SCC axis +H (shown in Fig. 1) with an axis perpendicular to the planes of the top and bottom field-generating coils. From this position, the monkey was reoriented via a 45 ° yaw within the field coil frame so that the +LARP and +RALP SCC axes aligned with the axes of the other two pairs of field-generating coils. The three fields generated by the coils were therefore orthogonal to each other and approximately aligned with mean SCC axes.

The chair was mounted atop an Earth-vertical axis rotator within a gimbal that allowed us to reorient the animal and field coils en bloc to align the +H, +LARP, or +RALP SCC axes with the Earth-vertical axis of the rotator. Yaw rotation about the +H axis was delivered with the animal erect; a clockwise motor rotation (as viewed from above) excited the right horizontal SCC while inhibiting the left horizontal SCC. LARP axis rotations were delivered with the gimbal reoriented to position the animal's torso supine after its head was first reoriented to turn the nose 45 ° toward the left ear; in this orientation, a clockwise (viewed from above) motor rotation excited the left anterior SCC and inhibited the right posterior SCC. RALP axis rotations were delivered with the animal's torso positioned supine after its head was first reoriented to turn the nose 45° toward the right ear; a clockwise (viewed from above) motor rotation excited the left posterior SCC and inhibited the right anterior SCC. Unless otherwise noted, the polarity of eye velocity traces in all figures is kept consistent with a right-hand rule (with positive yaw, LARP, and RALP eye movements resulting from excitation of the right horizontal, LA, and LP canals, respectively (Migliaccio et al. 2004)), while head velocity traces are inverted when needed to compare to the eye movement responses they elicit.

The three frequency signals induced in each scleral coil were demodulated to produce three voltages proportional to the angles between each coil and each magnetic field then analyzed using 3D rotational kinematic methods detailed by Straumann et al. (1995). All signals encoding motion of the head or the eye were passed through an eight-pole Butterworth anti-aliasing filters with a corner frequency of 100 Hz prior to sampling at 200 Hz. Coil misalignment was corrected using an algorithm that calculated the instantaneous rotational position of the coil pair with reference to its orientation when the eye was in a reference position (Tweed et al. 1990). Angular rotations were expressed as rotation vectors with LARP, RALP, and H coordinates with regard to the SCC-based coordinate system (Fig. 1), and the angular velocity vectors of eye with respect to head were calculated from the corresponding rotation vectors (Haslwanter 1995; Migliaccio et al. 2004; Hepp 1990). Briefly, we computed eye recoil frame angular position and angular velocity using rotation matrices, rotation vectors, and quaternions, transforming between these representations as required for computational efficiency using algebraic formulae well described in reviews and textbooks on rotational kinematics (e.g., Haslwanter 1995; Migliaccio et al. 2004). We took the plane perpendicular to the head restraint's axis as the mean horizontal SCC plane, and we approximated the mean LARP and RALP planes as being perpendicular to the mean horizontal SCC plane and 45 ° from the interaural axis. Angular position resolution of the coil system was 0.2 ° (tested over the angular range of ±25 ° combined yaw, pitch, and roll positions), and angular velocity noise was ~2.5 °/s peak.

For responses to sinusoidal stimuli, each of the three eye movement components (horizontal, LARP, and RALP) was separately averaged for 10–20 cycles free of saccades and blinks. For each component of each sinusoidal stimulus and corresponding response,

we used a single-frequency Fourier analysis to compute the magnitude of the single, symmetric best-fit sinusoid to the response, under the constraint that the response frequency was the same as the known stimulus frequency. In every case, the fraction of signal energy (i.e., variance integrated over all cycles) not accounted for by the best-fit sinusoid was <15 %. We also computed half-cycle gains by repeating the fitting procedure with only positive or only negative stimulus half cycles to determine VOR gain asymmetry (the ratio of excitatory/inhibitory half cycle gain)

VOR misalignment angle was computed as the four-quadrant arccosine (in degrees) of the dot product between two unit vectors describing the ideal and actual VOR response eye rotation axes as measured at the time of the peak velocity of the component about the axis of the predominantly excited SCC. These two vectors were never more than 90 ° apart, so misalignment was always a positive number prior to averaging.

For responses to transient whole-body rotations, we quantified VOR gain using "acceleration segment gain" G_A, which is the mean ratio of eye/head speed about the axis of head rotation computed during the 1,000 °/s^2 constant acceleration segment of the stimulus (Migliaccio et al. 2004). For each trial, response latency was computed as the time difference between the zero-velocity intercept times for the best-fit lines approximating the constant acceleration segment of mean eye and head velocity traces. These times were measured using the iterative linear fit method described in Migliaccio et al. 2004. To compare VOR gains, phases, G_A values and latencies across animals, status (normal, BVD/implanted/nonmodulated, BVD/implanted/modulated), frequencies, SCC axes, and rotation half cycles, we used ANOVA followed when indicated by post hoc *t* tests, with $P<0.05$ considered significant.

We defined VOR gain asymmetry α for head and eye rotations about each SCC axis as the quantity $\alpha=(G_E-G_I)/(G_E+G_I)$, where G_E denotes VOR gain in response to head rotations that are excitatory for the left, implanted labyrinth (e.g., leftward for yaw rotations; simultaneously rolling top of head toward left ear while pitching it toward the nose LARP rotations; and simultaneously rolling top of head toward left ear while pitching it away from the nose for RALP rotations) and G_I denotes VOR gain for the opposite sense of head rotation about the same axis. For sinusoidal stimuli, G_E and G_I were half-cycle gains; for transient stimuli, G_E and G_I were the G_A values for excitatory and inhibitory rotations, respectively.

To compare VOR gains across animals, frequencies, SCC axes, and rotation half cycles, we used MATLAB (MathWorks, Natick, MA) to perform ANOVA followed when indicated by post hoc *t* tests, with $P<0.05$ considered significant. Standard deviations are computed across cycles for a given animal and across the mean value (over many cycles) for each animal when aggregated as data points across animals.

Prosthetic stimulation paradigm

We mounted the prosthesis in the plastic cylinder chamber atop the head, taking care to align all three gyroscopes with their respective mean SCC planes. To power the prosthesis, we used three 3.4-V lithium ion batteries in parallel so that batteries could be replaced without interrupting power delivery.

Prior to commencing the adaptation trial, we measured 3D VOR responses to head rotation in darkness with the MVP powered on but firing only at baseline rates that did not modulate with head motion. We then programmed the MVP to sense 3D head angular velocity and accordingly modulate the pulse rate of charge balanced, symmetric, biphasic current pulses delivered to each SCC's ampullary nerve. We determined the stimulation current amplitude for each electrode by gradually increasing the current amplitude of 200 μs/phase pulses frequency modulated over 0–200 pulse/s (pps) at 1 Hz while we measured 3D eye velocity. For adaptation experiments, we set the stimulus current for each electrode at the level that evoked a midrange eye velocity without eliciting signs of facial nerve activation. This typically corresponded to a stimulus current amplitude at which the 3D axis of VOR responses for stimulation on a given SCC's electrode on day 1 was not perfectly aligned with that SCC's axis. Table 1 shows the stimulation currents used for each electrode.

After we identified the optimal electrode current amplitude and set it as a constant for each stimulation channel, we determined a "mapping function" for each SCC, by which head angular velocity about that SCC's axis would be transformed into changes in stimulus pulse frequency (Chiang et al. 2011). We used 94 pps baseline stimulation rate, peak rate of 300 pps, and a sigmoid curvature of $C=2$ (Della Santina et al. 2007) to mimic the mean resting rate of normal rhesus monkey vestibular afferent fibers (Sadeghi et al. 2007). In chinchillas, the mean resting rate after intratympanic gentamicin treatment is typically about 60 % of normal (Hirvonen et al. 2005; Della Santina et al. 2005b), so the 94-pps baseline rate is probably above the spontaneous rate in rhesus monkeys after gentamicin ototoxic injury.

As described in detail in previous publications (Dai et al. 2011; Chiang et al. 2011; Della Santina et al. 2007; Davidovics et al. 2013), the mapping function

TABLE 1

Stimulation current levels (microampere per phase) used for each active electrode in each animal

Monkey ID	*Electrode*	*μA/phase*
F247RhE	LH	65
	LA	75
	LP	85
F234RhD	LH	110
	LA	80
	LP	100
F20124RhB	LH	90
	LA	100
	LP	100
M067RhF	LH	100
	LA	135
	LP	122
F60738RhG	LH	120
	LA	120
	LP	120

LA, LH, and LP = active electrode's target ampullary nerve (Left Anterior, Left Horizontal, and Left Posterior, respectively). Electrode in common crus was used as a reference. Amplitudes were determined at the beginning of the recording session and kept constant for the duration of that experiment

was sigmoidal, smooth, and approximately linear for small deviations about the baseline pulse rate of 94 pps. The maximum pulse rate (e.g., during excitatory head rotations at >300 °/s) was 400 pps, and the minimum pulse rate (e.g., during inhibitory head rotations at >300 °/s) was 0 pps. Since there is greater "head room" for increasing the rate than for decreasing it, the relationship between head velocity and pulse rate necessarily included a lower mean sensitivity (in pulse per second per degree per second) for inhibitory head rotations than for excitatory head rotations.

The adaptation experiments were performed 6 to10 weeks after electrode implantation. Prior to the start of this study of continuous/chronic adaptation, each animal was subjected to multiple brief episodes of electrical stimulation during acute measurements to determine optimal stimulation parameters. For all figures showing responses to continual/chronic stimulation, "day 1" signifies measurements taken in the first 2–4 h after the onset of continual/chronic stimulation. During that 2–4 h, the animal sat stationary in a chair with the head and visual surround fixed and the pulse rate constant at the baseline rate. During testing, animals were in complete darkness. In between measurement sessions, each monkey resided in its home cage where it was free to move normally under diurnal lighting conditions while continuing to receive head motion-modulated stimulation. We did not present rewards for behavior.

RESULTS

VOR responses to sinusoids

Figure 2A–C shows mean cycle-averaged head and eye angular velocities of a normal rhesus monkey (F234RhD) during 20 cycles of 1 Hz, 50 °/s peak passive, sinusoidal whole-body rotations in darkness about the mean horizontal (top row), LARP (middle row), and RALP (bottom row) SCC axes. When a normal rhesus monkey was rotated sinusoidally at 1 Hz, 50 °/s peak in darkness, the eyes responded by moving in the direction opposite the rotation of the head at approximately the same velocity of the head motion. The pulse rate of MVP in response to a 50 °/s head velocity is 130~205 pulse/s with a baseline of 94 pulse/s. The mean gain for the main VOR component (i.e., about the axis of head rotation) was 0.94± 0.12, 0.86±0.14, and 0.82±0.17 (mean ± SD, N=10–20 cycles) for rotations about the horizontal, LARP, and RALP axes, respectively. Components about other axes were relatively small, indicating a well-aligned 3D VOR response.

Figure 2D–F shows responses during the same whole-body motion stimuli for a monkey treated bilaterally with gentamicin, implanted with MVP electrodes on the left side, and stimulated with a prosthesis set to fire at a constant baseline pulse rate while ignoring the head rotation signals reported by its gyro sensors (Dai et al. 2011). Under this condition, the 3D VOR response was profoundly deficient, making the degree of VOR misalignment hard to quantify.

Eye movement responses recorded during whole-body rotation with motion-modulated MVP stimuli within 4–6 h of initial activation of MVP gyro-driven modulation were already aligned somewhat with head rotation axes, but significant misalignment was still evident in the form of nonzero response components about axes other than the axis of head rotation (Fig. 2G–I). For example, when the animal's head was rotated about the +H axis, the eyes responded primarily by rotating about the +H axis, but substantial LARP and RALP components were also present (Fig. 2G). By the seventh day after MVP activation, LARP and RALP components of the eye response to horizontal whole-body rotation were substantially attenuated, while the horizontal component remained nearly constant (Fig. 2M). A similar improvement in misalignment was evident on the third and the seventh days of stimulation when this animal was tested by rotating it about the LARP (Fig. 2H, K, N) and RALP (Fig. 2I, L, O) axes. This progressive improvement in misalignment is illustrated in spherical polar form for a second animal in Figure 3, which shows how the mean 3D axis of eye rotation evolves over 7 days of prosthesis use. The direction and peak magnitude of VOR eye movement responses to head

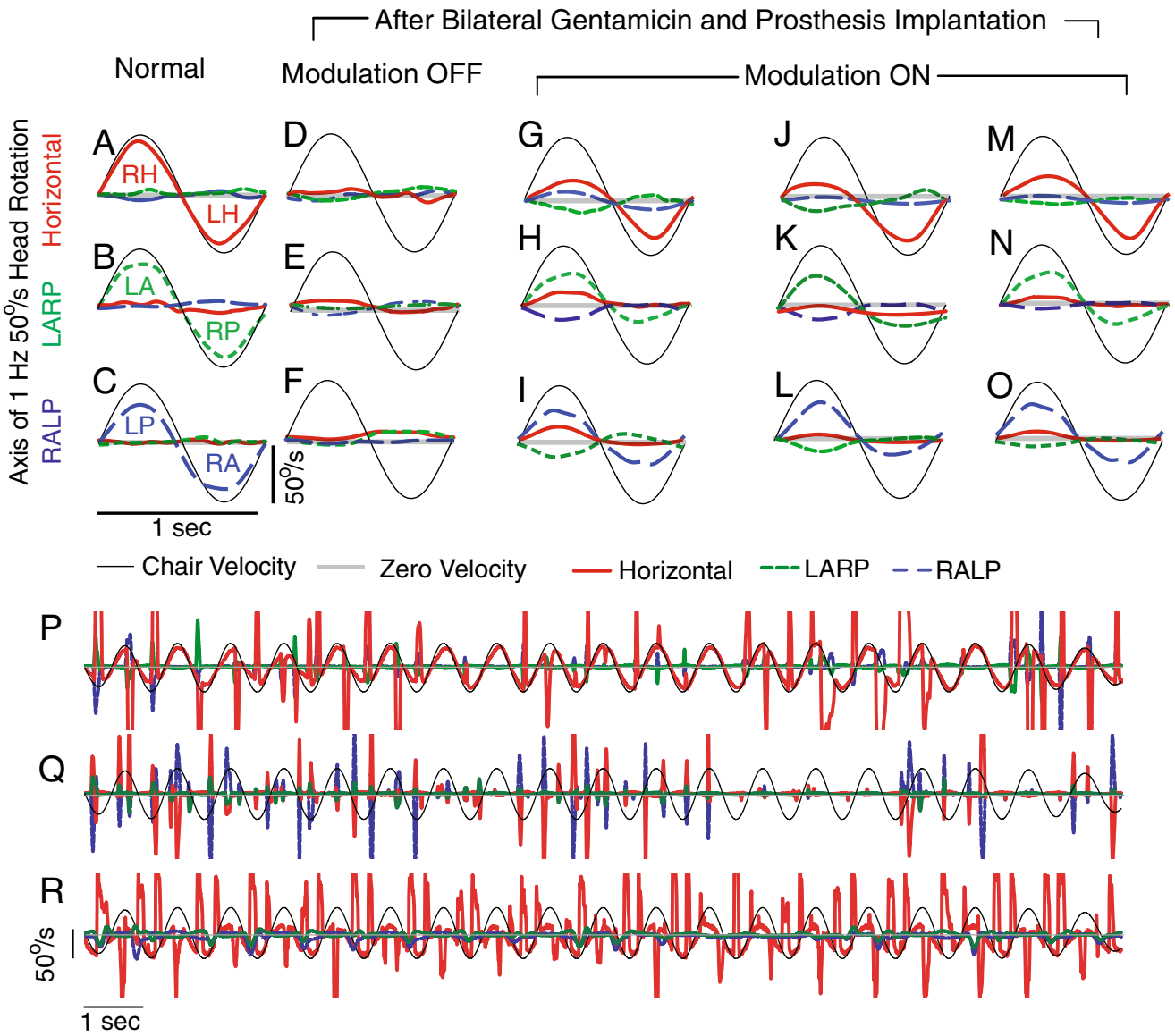

FIG. 2. Mean 3D VOR eye responses of a rhesus monkey (F234RhD) during actual 50 °/s peak, 1 Hz, passive whole-body rotations measured in darkness 2 h after onset on of chronic, continuous motion-modulated stimulation on day 1 of the adaptation paradigm. **A–C** Normal responses before gentamicin treatment and MVP implantation, during rotations predominantly exciting the left and right horizontal (*LH* and *RH*, **A**), left anterior/right posterior (*LARP*, **B**), and right anterior/left posterior (*RALP*, **C**) canals. In each case, horizontal, LARP, and RALP components of the 3D VOR response are shown in *red/solid*, *green/dashed*, and *blue/long dash lines*, respectively, and the canal being excited during a given half cycle is designated. (By the right-hand rule convention used to describe 3D eye movements, VOR responses to LH excitation are negative, whereas responses to LA and LP excitation are positive.) **D–F** Responses to whole-body rotation measured after gentamicin and multichannel vestibular prosthesis (MVP) electrode implantation, with the MVP set to pulse at constant rates independent of head motion. **G–O** 3D VOR responses measured on the first day of continuous motion-modulated MVP stimulation (**G–I**), third day (**J–L**), and seventh day (**M–O**). Each panel shows mean of 10–20 cycles free of quick phases. SD<5 °/s at every time point for every trace. **P–R** Cycle to cycle variation for the measurements shown in mean form in **A**, **D**, and **M**.

rotations about each of the three mean anatomic SCC axes approached ideal eye responses over time.

This improvement over time in encoding of head movement axis was evident for all four rhesus monkeys studied, for all three axes of head rotation tested. Figure 4 shows the amplitude of each eye rotation component during sinusoidal 1 Hz, 50°/s peak horizontal, LARP, and RALP whole-body head rotations in darkness for each of the four rhesus monkeys individually. Figure 5 shows the amplitude of

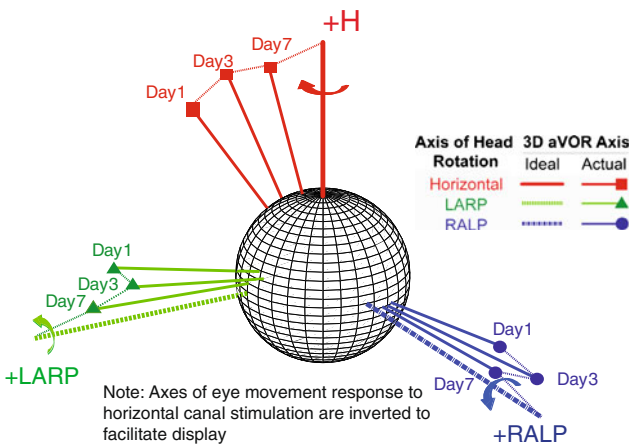

FIG. 3. Changes in axis of eye response for one rhesus monkey (F234RhD) over 7 days of continual motion-modulated stimulation. Each data vector depicts the 3D axis and magnitude of VOR responses during whole-body, 1 Hz, 50 °/s peak head rotations in darkness about the mean horizontal, LARP, and RALP semicircular canal axes. *Vector length* indicates the peak response velocity; for comparison, *thick axes* without markers depict inverse of 50 °/s peak head rotations about each canal axis. Data shown are for peak excitatory responses; *curved arrows* in inset show the direction of VOR response to excitation of the corresponding semicircular canal in the left labyrinth. Axes for responses to left horizontal SCC excitation are inverted to facilitate consolidation on a single plot, and the direction of rotation indicated by the *red arrow* is the rightward yaw rotation resulting from left horizontal SCC excitation. Progression over time toward the ideal response is apparent for each axis of head rotation. Each data vector shown on the plot has both a direction and a magnitude, conveying the axis and relative amplitude, respectively, of the VOR response.

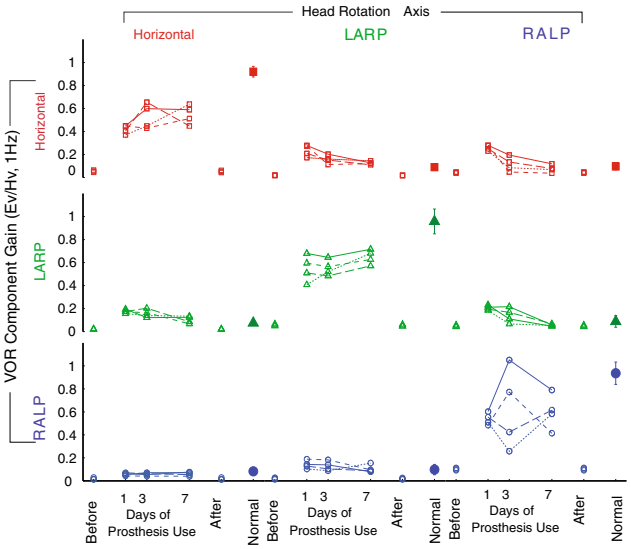

FIG. 4. Gain of each component of 3D VOR responses for each of $N=4$ monkeys during 1 Hz, 50 °/s, peak whole-body rotations about the horizontal, LARP, and RALP canal axes on the first, third, and seventh days of continuous stimulation using a head-mounted multichannel vestibular prosthesis. *Before*: values for each monkey measured in response to head movement with the prosthesis stimulating at constant pulse rates, independent of head velocity, 3–5 h after prosthesis activation. *After*: values measured 4–48 h after the prosthesis was powered off on day 7. Normal: Mean ± SD responses of five normal rhesus monkeys. *Ev* eye velocity; *Hv* head velocity.

each eye rotation component during sinusoidal 1 Hz, 50 °/s peak horizontal, LARP, and RALP whole-body head rotations in darkness individually for each of the four prosthesis animals. In every monkey, the component of 3D eye rotation about the head rotation axis (i.e., the desired response) remained nearly constant (i.e., did not significantly change, despite a trend toward increasing) for the first, third, and seventh days of continual prosthesis use, except for increased variability in RALP responses on day 3, while the relative amplitude of each undesired off-axis component progressively and consistently decreased, so that responses on day 7 of prosthetic stimulation were significantly more similar to normal responses than on day 1 (two-way ANOVA with factors *animal* and *day*: $F=5.21$, $P=0.0071$ for yaw, LARP, and RALP head rotation).

To ensure that this marked improvement was not due to recovery of hair cell function, we measured responses again with the prosthesis power turned off on day 7. Without prosthesis stimulation, VOR responses were again consistent with profound bilateral hypofunction (very low gains in all VOR components), confirming that all responses and improvement observed during the 7-day trial depended on prosthetic input.

Improvement in 3D VOR axis alignment was evident for every sinusoidal stimulus frequency examined. Figure 6 shows VOR gain (top), phase (middle row), and 3D axis misalignment angle (bottom) for different frequencies and axes of head rotation averaged for each of four rhesus monkeys. For each of the frequencies tested, the gain of the eye responses remained relatively high and over all significantly increased ($F(3,20)=2.94$, $P=0.027$), phase did not change significantly over time (two-way ANOVA, $F(1, 8)=3.24$, $P=0.1151$), and directional misalignment between the 3D VOR response and the axis of head rotation significantly improved over the seven days of prosthetic stimulation (two-way ANOVA, $F(1, 8)=2.85$, $P=0.0017$). As evident in Figure 6, this pattern was consistent for every animal.

Asymmetry of VOR responses to sinusoids

In normal monkeys before MVP implantation and gentamicin treatments, VOR asymmetry was near zero (Fig. 7). After bilateral gentamicin treatment, left MVP implantation, and MVP activation in normal gyro-modulated mode, substantial VOR asymmetry was observed in responses during motion-modulated MVP-induced response at day 1 (Figs. 2G–I and 6), with asymmetry $\alpha \sim 0.4$. After 7 days of continuous stimulation, the change in VOR asymmetry from day 1 to day 7

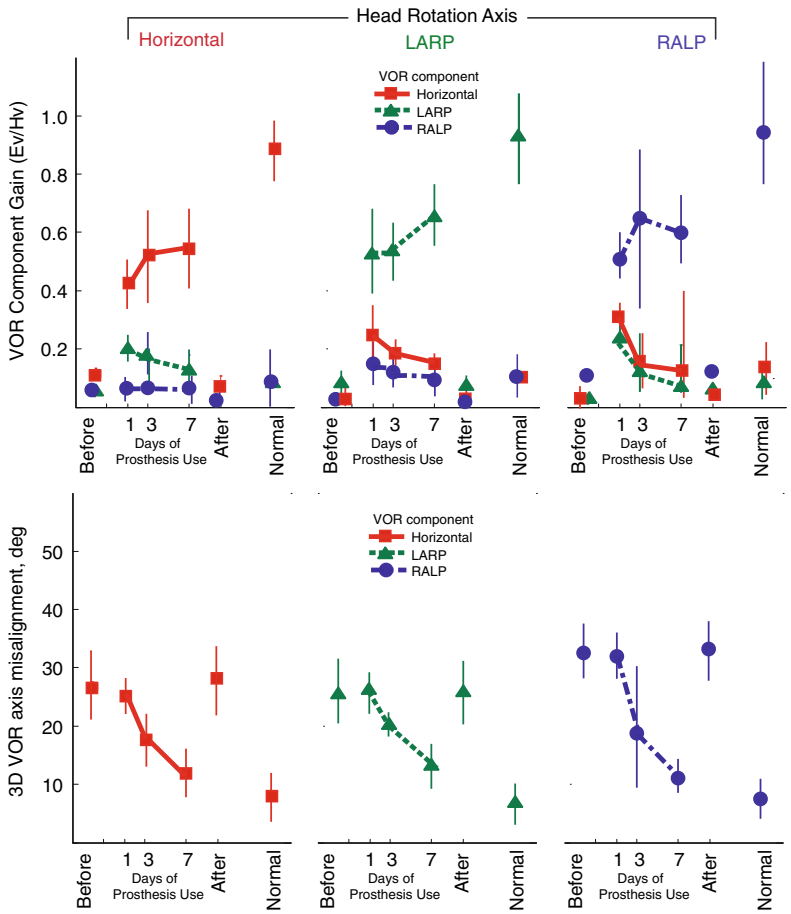

FIG. 5. Mean ± SD gain (*top*) and eye/head 3D axis misalignment angle (*bottom*) for N=4 rhesus monkeys, displayed for each component of the peak 3D VOR eye movement response during 50 °/s peak whole-body rotations in darkness at 1 Hz about the horizontal, LARP, and RALP canal axes on the first, third, and seventh days of continuous stimulation using a head-mounted multichannel vestibular prosthesis. The 3D VOR response maintained gain of the desired component while improving directional misalignment over 7 days of continuous prosthesis for every stimulus frequency, axis, and animal examined. *Before:* values measured to head movement with the prosthesis stimulating at constant pulse rates, independent of head velocity, 3–5 h after prosthesis activation. *After:* values measured 4–48 h after the prosthesis was powered off on day 7. *Normal:* Responses of five normal rhesus monkeys. *Ev* eye velocity; *Hv* head velocity.

was not statistically significant (two-way ANOVA with factors animal and day, F=3.42, P=0.1151), although data did trend toward slight improvement over time.

The offset eye velocity (i.e., DC component of a best-fit sinusoid with DC offset) during stimulation at 0 head velocity was ≤8 °/s for all monkeys in the day 1 measurement (in darkness 2 to 4 h after initial activation, with the animal head fixed in light amid a stationary visual surround during that 2–4 h) and was smaller on days 3 and 7.

VOR responses to transient head rotations

Normal responses. The G_A, latency, and asymmetry of VOR responses to transient head rotations in darkness for these four animals when normal (prior to gentamicin treatment), BVD (after bilateral gentamicin treatment and unilateral electrode array implantation but with only nonmodulated stimulation), and on the first day of prosthesis activation have been previously described elsewhere as part of a study including a fifth animal not subjected to chronic stimulation (Dai et al. 2011). As reported in that study, the mean G_A for the VOR component about the axis of head rotation is symmetric for normal rhesus monkeys for either rotation sense about each axis and, for stimuli exciting the left labyrinth, is equal to 0.98±0.04, 0.93±0.05, and 0.99±0.04 for rotations about the horizontal, LARP, and RALP axes, respectively. Components about other axes are small, indicating a well-aligned 3D VOR. The mean response latency is also symmetric and is equal to 8.4±1.4, 9.5±3.4, and 9.3±0.9 ms for rotations about the horizontal, LARP, and RALP axes, respectively.

BVD with nonmodulated MVP input. As previously reported (Dai et al. 2011), mean G_A and response latencies pooled for both sides and across four BVD monkeys for rotations about each SCC axis during nonmodulated MVP stimulation are grossly deficient

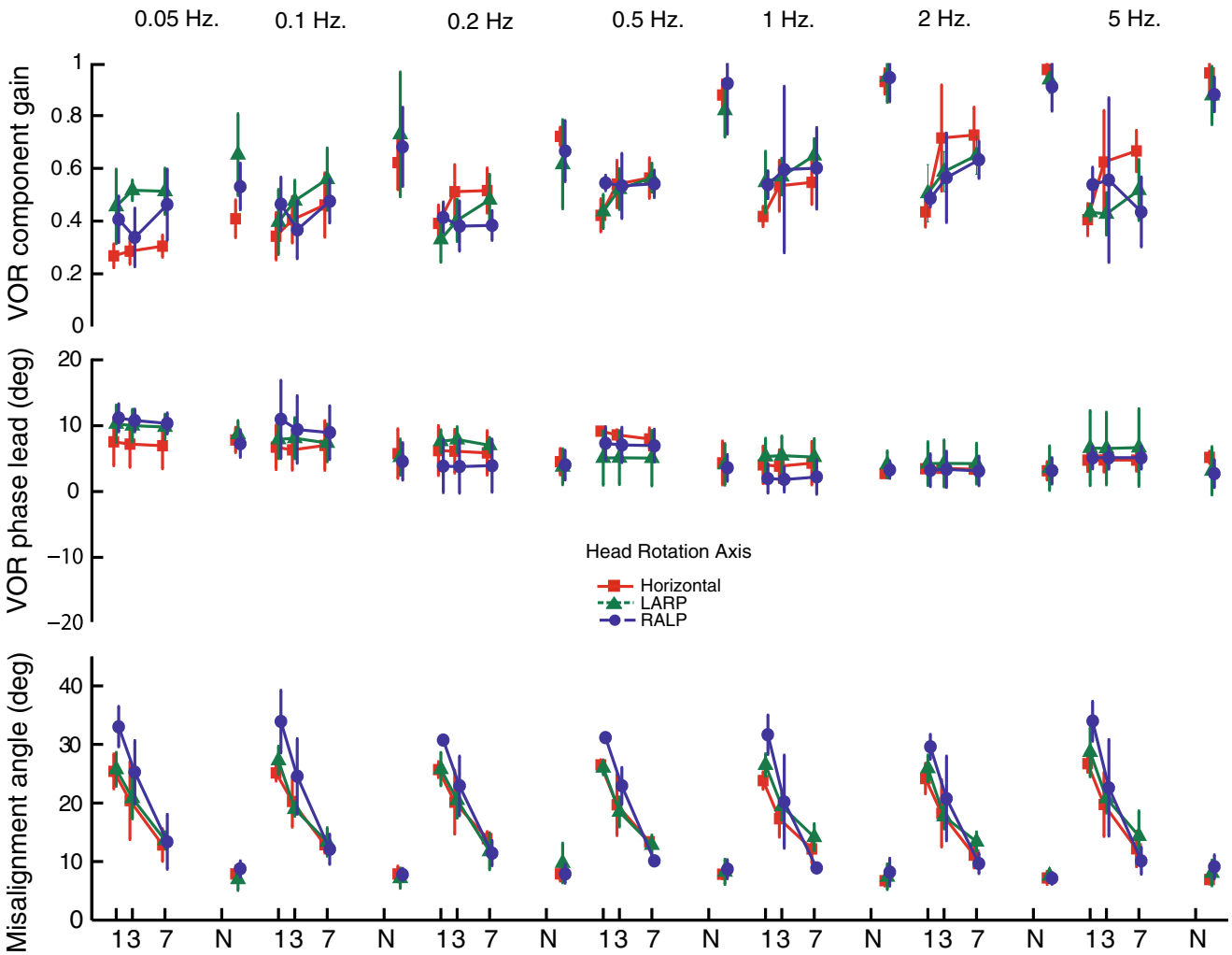

FIG. 6. Mean ± SD gain for the component of the 3D VOR about the axis of head rotation (*top*), phase lead versus inverse of head velocity (*middle*), and eye/head misalignment angle (*bottom*) for *N*= 4 rhesus monkeys, displayed for 3D VOR eye movement responses during 50 °/s peak whole-body rotations in darkness at 0.05–5 Hz about the horizontal (*square*), LARP (*triangle*), and RALP (*circle*) canal axes on the first, third, and seventh days of continuous stimulation using a head-mounted multichannel vestibular prosthesis. In each case, gain is the ratio [(peak velocity of the VOR component about the axis of head rotation)/(peak velocity of whole-body rotation)], phase is expressed in degrees by which a best-fit sinusoid approximating the inverted eye velocity response's main component leads a best-fit sinusoid fit to the head velocity, and misalignment is the angle between 3D vectors describing the actual and desired axes of 3D VOR eye movement response at the time of peak eye velocity. The 3D VOR response maintained gain of the desired component while phase did not significantly change and misalignment significantly improved over 7 days of continuous prosthesis for every stimulus frequency, axis, and animal examined. *N* normal.

in all directions during acceleration steps, with G_A averaging 0.10±0.04, 0.11±0.02, and 0.18±0.02 for H, LARP, and RALP, rotations, respectively, while latency is prolonged to 15.10±5.47, 15.28±3.52, and 14.83± 2.42 ms. A multiway ANOVA revealed that G_A is significantly lower (P=0.0051; F=10.20, F_{crit}=5.32), and the latency is significantly longer (P=0.0308; F=8.12, F_{crit}=5.32) compared to normal.

Changes over time after MVP activation. As for sinusoidal VOR responses, substantial improvement of misalignment was observed in VOR responses to 1,000 °/s^2 transient whole-body rotations after 1 week of continuous motion-modulated prosthetic stimulation, while asymmetry did not significantly change. Figure 8A–C shows cycle-averaged responses for normal monkey F234RhD during acceleration steps before electrode implantation and gentamicin treatment. Components about axes other than the head rotation axis were small relative to the main component, indicating a well-aligned 3D VOR. Figure 8D–F shows cycle-averaged head and eye angular velocities of monkey F234RhD after bilateral gentamicin treatment and left MVP implantation, during MVP stimulation with only a constant baseline rate. The mean G_A for the VOR component about the axis of head rotation was small for rotations

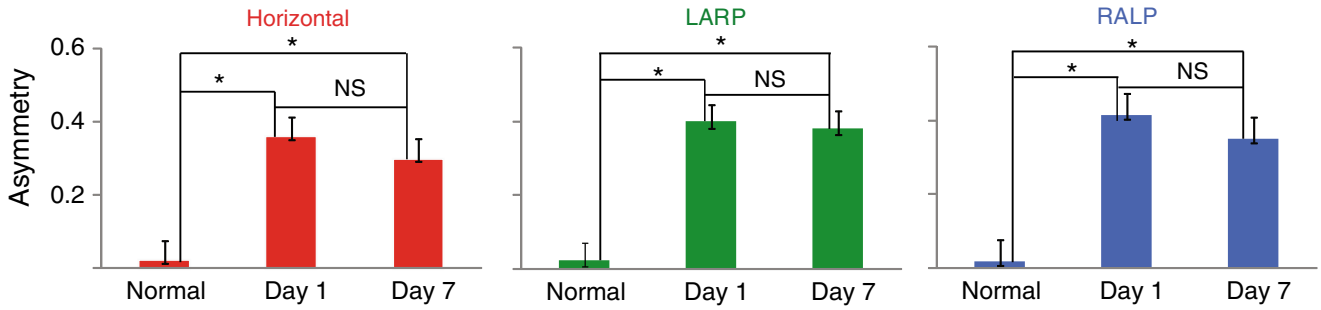

FIG. 7. Mean ± SD asymmetry of VOR responses to actual 50 °/s peak, 1 Hz, passive whole-body rotations in darkness. We quantified gain asymmetry for VOR response by computing the ratio between the excitatory peak versus inhibitory peak difference in gain and the average gain, $\alpha=(G_E-G_I)/(G_E+G_I)$. This asymmetry is significantly reduced after the training ($P>0.05$, ANOVA). *Left* normal; *middle* first day; *right* seventh day. *Asterisk*, significant in Student's *t* test, $P<0.05$; *NS* nonsignificant, $P>0.05$.

about any axis, indicating a grossly deficient 3D VOR response with gains so low that response latency and axis are difficult to quantify. Figure 8G–I shows cycle-averaged responses after MVP motion modulation was on for 6 h on day 1. Mean G_A for the VOR component about the axis of head rotation was significantly larger than in Figure 8D–F, but other components were also larger. Figure 8M–O demonstrates alignment improvement during acceleration steps over 1 week of continuous stimulation. Despite this improvement in VOR gain and misalignment, asymmetry of responses to excitatory and inhibitory head rotations is still evident.

The latency of VOR responses did not change over time significantly (two-way ANOVA with factors animal and day, $F(1, 8)=4.23$, $P=0.1524$), but it did trend slightly downward over 7 days of stimulation (horizontal: from 10.6±2.3 to 10.1±1.8 ms; LARP: from 11.0±3.1 to 10.7±2.4 ms; RALP: from 10.4±1.4 to 9.9±1.7 ms).

DISCUSSION

Previous experiments have shown that misalignment between the actual axis of head motion and the perceived axis (as indicated by the VOR axis) occurs during prosthetic electrical stimulation of ampullary nerves, probably due to current spread (Della Santina et al. 2007; Lewis et al. 2010; Fridman et al. 2010; Hayden et al. 2011). Here, we examined whether misalignment can be reduced through central adaptation via a directional plasticity mechanism similar to that which arises when normal animals are exposed to directionally altered visual scene movement coupled to head rotation. We found that 3D angular VOR misalignment improved significantly with increasing duration of continuous prosthesis use. Eye versus head VOR misalignment during whole-body rotations about each of the three SCC axes in darkness decreased from ~30 ° to 50 ° on the day of prosthesis activation to ~10–20 ° after 7 days of continuous prosthesis use. This effect was observed at all frequencies tested. We conclude that, as might be expected from classic experiments eliciting VOR cross-axis adaptation in normal animals (e.g., Schultheis and Robinson 1981; Fukushima et al. 1996), sufficient plasticity exists in the vestibulo-ocular central nervous system to correct for errors in axis alignment due to abnormalities of the vestibular nerve activation pattern evoked by prosthetic electrical stimulation.

These findings demonstrate that the central nervous system rapidly adapts to multichannel prosthetic stimulation, markedly improving 3D VOR alignment during the first week after MVP activation in nonhuman primates. When combined with optimized electrode array design, surgical placement of electrodes as close to their target ampullary nerves as possible, optimal stimulus waveforms (Davidovics et al. 2011), and algorithmic approaches to correcting 3D misalignment (e.g., via linear algebraic manipulation of the gyro-stimulator mapping; Fridman et al. 2010), directional plasticity mechanisms can achieve well-aligned responses within 1 week of MVP activation. A similar process with a similar time course is likely to occur in humans.

Comparison to prior studies of prosthetic VOR alignment

The time course and extent of directional plasticity observed in the present study were consistent with previous studies of cross-axis adaptation in normal

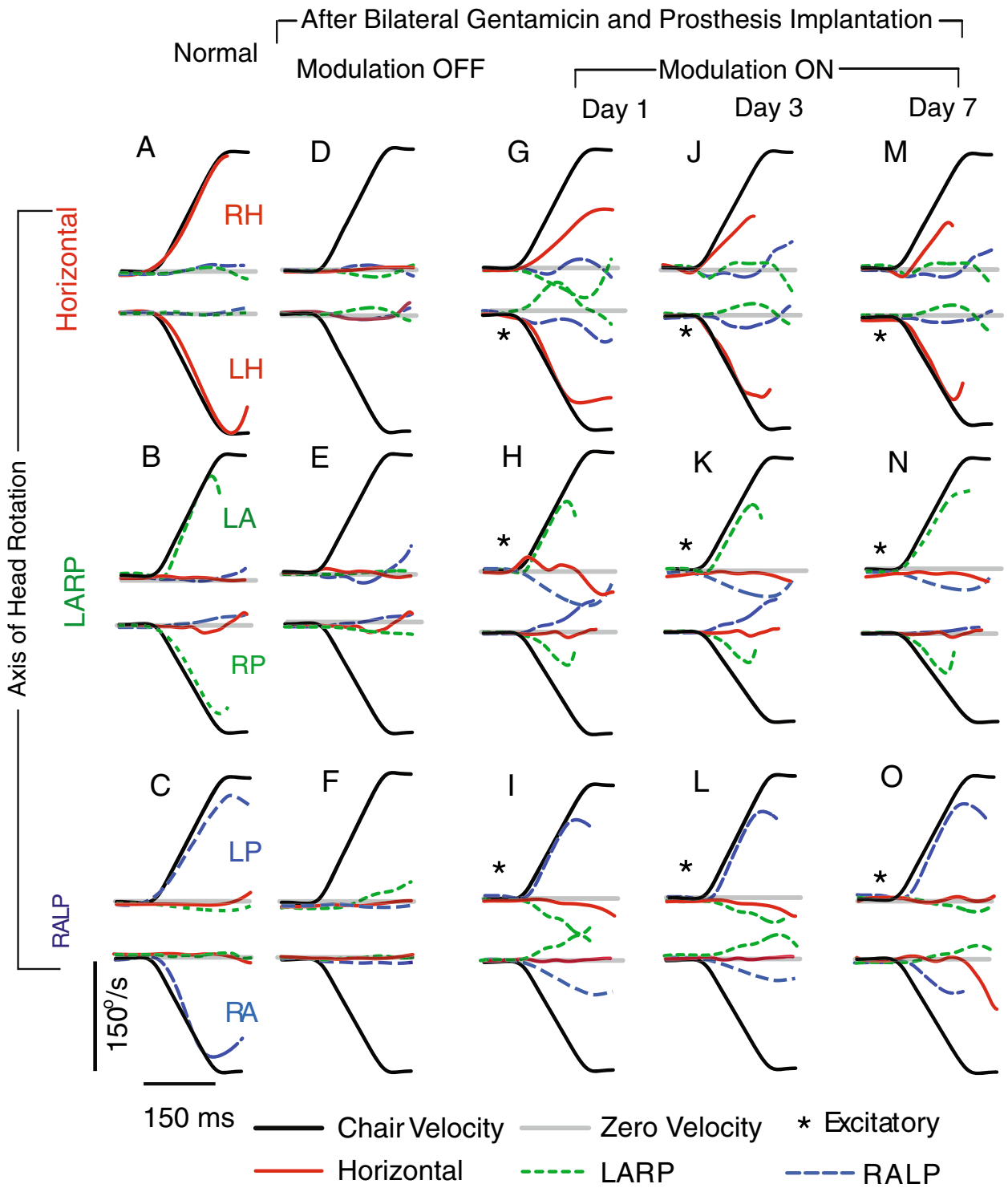

FIG. 8. **A–C** Mean ± SD eye and (*inverted*) head angular velocities of a normal rhesus monkey (F234RhD) during head impulse rotations (1,000 °/s^2 to a peak head velocity of 150 °/s) in darkness, about the horizontal (**A**), left anterior/right posterior (*LARP*, **B**), and right anterior/left posterior (*RALP*, **C**) semicircular canal axes. Standard deviation of each trace at each time point is <10 °/s. Data are truncated at the onset of the first nystagmus quick phase. **D–F** Same monkey (F234RhD) after bilateral intratympanic gentamicin and electrode implantation in left labyrinth, with MVP pulsing at baseline stimulation rate of 94 pulses/s on each channel but not modulating with head rotation. Responses are minimal, indicating failure of the VOR. **G–I** Same animal with motion-modulated MVP input at first day of MVP modulation on. **J–L** Third day response with improvement of misalignment. **M–O** Seventh day response with further improvement of misalignment, but not significant improvement of asymmetry (P>0.05). Head movement traces are inverted for comparison to eye data. *Asterisks* indicate head rotations that excite the left labyrinth. (By the convention used to describe 3D movements, rightward eye movements are negative, while responses to exciting the LA and LP SCCs are positive).

cats exposed to abnormal visual input (e.g., Schultheis and Robinson 1981) and gain adaptation in labyrinthectomized rhesus monkeys (Sadeghi et al. 2010).

Compared with similar experiments conducted in chinchillas (Dai et al. 2011), the initial misalignment in rhesus monkeys was less and the reduction of misalignment after 7 days stimulation was greater. Reasons for the more favorable results in monkeys could include increased relative precision of electrode placement in the larger rhesus labyrinth, improved surgical technique, greater separation of nontarget nerve branches from an active electrode, and differences in 3D VOR gain anisotropy between chinchillas (which have a relatively isotropic but weak VOR) and rhesus monkeys (which have nearly ideal horizontal and pitch VOR gains but relatively weak VOR gain for roll head rotations) (Migliaccio et al. 2004).

There are no published prior studies of 3D VOR directional plasticity in rhesus monkeys using a multichannel vestibular prosthesis; however, relevant data are available for squirrel monkeys using a single-channel head-mounted vestibular prosthesis aligned with the horizontal or posterior SCC (Lewis et al. 2002, 2010). In those studies, alternating between high and low sensitivity mappings of head velocity to pulse rate improved gain (from 0.11 to 0.17) and 2D VOR misalignment toward the desired responses to yaw head rotations (i.e., a ~30 ° shift from mostly pitch to mostly yaw; roll was not measured) over 20–60 days of continual prosthesis use.

Although direct comparison between the present study's 3D results in rhesus monkeys and the Lewis et al. studies' 2D results in squirrel monkeys is complicated by differences in stimulation protocol and measurement technique, it appears that 3D VOR realignment in the present study's rhesus monkeys receiving three-channel MVP stimulation was similar to but faster than responses measured by Lewis et al. for squirrel monkeys receiving single-channel stimulation. Repeating the single-channel stimulation of Lewis et al. in rhesus monkeys could help to determine whether the apparently faster directional plasticity observed in the present study is primarily due to interspecies differences (which seems unlikely given similarity of VOR physiology across primates) or to the fact that multichannel stimulation provides more information to the vestibular central nervous system (and thus, a more congruent driving signal to engender directional plasticity mechanisms [Dai et al. 2011]).

Changes in 3D VOR asymmetry

Bilateral vestibular prostheses acting in complementary fashion can achieve more symmetric VOR responses than a unilaterally implanted device, at least in the short term (Gong et al. 2008). However, considering the risks and costs of bilateral device implantation, reducing asymmetry of the VOR induced by unilateral stimulation is a key goal in advancing application of a MVP that restores VOR by stimulating a vestibular nerve in patients suffering from bilateral loss of vestibular sensation.

Using baseline MVP stimulation rates above the mean spontaneous rate of gentamicin-treated afferents allows both upward and downward modulation of pulse rate. This should achieve more symmetric responses for both excitatory and inhibitory head rotations, respectively, in an animal using a single, unilaterally implanted prosthesis, than could be achieved without a baseline rate above the afferents' spontaneous discharge. By adapting central vestibular neurons to an increased baseline rate when the head is stationary, one can down-modulate stimulus pulse rates further below baseline to encode inhibitory head rotations (e.g., see Lewis et al. 2010; Della Santina et al. 2007; Davidovics et al. 2011). In this study, we used approximately normal baseline rates in the MVP, accepting a greater degree of VOR asymmetry (because spontaneous afferent activity maintains a floor beneath which reductions in prosthesis pulse rate cannot reduce afferent activity; in exchange for a larger dynamic range of eye rotations in response to excitatory head rotations.

Unfortunately, we did not observe a significant improvement VOR asymmetry over 1 week of MVP stimulation. The "spontaneous" nystagmus caused by baseline stimulation (with the animal stationary in darkness after a 2–4-h period of adaptation while stationary in light with a visual surround) was ≤8 °/s in each animal on day 1 and reduced to 2–3 °/s in each animal by day 7; however, it did not reduce to zero. The asymmetry we observed during 50 °/s peak, 0.2–5 Hz head rotations on days 1–7 of chronic MVP stimulation in rhesus monkeys was similar to that exhibited by squirrel monkeys (Lasker et al. 2000) and humans (Furman et al. 1989) tested using similar head rotations during the first week of vestibular compensation following acute unilateral surgical deafferentation. It did not change significantly during the week of prosthesis use (Fig. 7). Whether the improvements we observed in 3D VOR alignment over the first week of unilateral MVP use will be accompanied by significant improvement in VOR asymmetry over a longer duration of MVP use remains to be seen.

Interestingly, recent evidence suggests that animals with stable asymmetric VOR gain deficits long after unilateral labyrinthectomy retain sufficient "adaptive reserve" to raise ipsilesional VOR gain nearly to normal if they are exposed to a training regimen comprising repeated whole-body rotations toward the lesioned side while wearing magnifying spectacles

(Minor and Lasker 2009; Ushio et al. 2011). Thus, a training paradigm that exposes an individual to retinal slip only for ipsilesional head rotations and never for contralesional head rotations might decouple ipsilesional and contralesional VOR gain adaptation sufficiently to allow selective enhancement of ipsilesional VOR gain. Whether such a training paradigm can improve asymmetry of the VOR driven by a unilaterally implanted MVP remains to be seen.

ACKNOWLEDGMENTS

We thank Lani Swarthout for assistance with animal care. This work was funded by NIH NIDCD grants R01DC009255, R01DC2390, and 5F32DC009917. CDS, GYF, and BC are inventors on pending and awarded patents relevant to prosthesis technology, and CDS is the CEO of and holds an equity interest in Labyrinth Devices LLC. We thank Lani Swarthout for assistance with animal care and Roland Hessler and Frank Risi for assistance with electrode array fabrication. The terms of these arrangements are being managed by the Johns Hopkins University in accordance with its conflict of interest policies.

REFERENCES

BAKER J, HARRISON RE, ISU N, WICKLAND C, PETERSON B (1986) Dynamics of adaptive change in vestibulo-ocular reflex direction. II. Sagittal plane rotations. Brain Res 371(1):166–170

BAKER JF, WICKLAND C, PETERSON B (1987) Dependence of cat vestibulo-ocular reflex direction adaptation on animal orientation during adaptation and rotation in darkness. Brain Res 408:339–343

BLACK FO, WADE SW, NASHNER LM (1996) What is the minimal vestibular function required for compensation? Am J Otol 17:401–409

CAREY JP, DELLA SANTINA CC (2010) Principles of applied vestibular physiology. In: Flint P (ed) Cummings otolaryngology: head and neck surgery. Elsevier, Amsterdam

CHIANG B, FRIDMAN GY, DAI C, RAHMAN MA, DELLA SANTINA CC (2011) Design and performance of a multichannel vestibular prosthesis that restores semicircular canal sensation in rhesus monkey. IEEE Trans Neural Syst Rehabil Eng 19(5):588–598

DAI C, FRIDMAN GY, DAVIDOVICS NS, CHIANG B, AHN JH, DELLA SANTINA CC (2011) Restoration of 3D vestibular sensation in rhesus monkeys using a multichannel vestibular prosthesis. Hear Res 281(1–2):74–83

DAVIDOVICS NS, FRIDMAN GY, CHIANG B, DELLA SANTINA CC (2011) Effects of biphasic current pulse frequency, amplitude, duration and interphase gap on eye movement responses to prosthetic electrical stimulation of the vestibular nerve. IEEE Trans Neural Syst Rehabil Eng 19(1):84–94

DAVIDOVICS NS, RAHMAN MA, DAI C, AHN JH, FRIDMAN GY, DELLA SANTINA CC (2013) Multichannel vestibular prosthesis employing modulation of pulse rate and current with alignment precompensation elicits improved VOR performance in monkeys. JARO 14(2):233–248

DELLA SANTINA CC, POTYAGAYLO V, MIGLIACCIO AA, MINOR LB, CAREY JP (2005A) Orientation of human semicircular canals measured by three-dimensional multiplanar CT reconstruction. JARO 6(3):191–206

DELLA SANTINA CC, MIGLIACCIO AA, PATEL AH (2005B) Electrical stimulation to restore vestibular function development of a 3-D vestibular prosthesis. Conf Proc IEEE Eng Med Biol Soc 7:7380–7385

DELLA SANTINA CC, MIGLIACCIO AA, PATEL AH (2007) A multichannel semicircular canal neural prosthesis using electrical stimulation to restore 3-D vestibular sensation. IEEE Trans Biomed Eng 54:1016–1030

DELLA SANTINA CC, MIGLIACCIO AA, HAYDEN R, MELVIN TA, FRIDMAN GY, CHIANG B, DAVIDOVICS NS, DAI C, CAREY JP, MINOR LB, ANDERSON ICW, PARK H, LYFORD-PIKE S, TANG S (2010) Current and future management of bilateral loss of vestibular sensation—an update on the Johns Hopkins Multichannel Vestibular Prosthesis Project. Cochlear Implants Int 11(s2):2–11

FRIDMAN GY, DAVIDOVICS NS, DAI C, DELLA SANTINA CC (2010) Vestibulo-ocular reflex responses to a multichannel vestibular prosthesis incorporating a 3D coordinate transformation for correction of misalignment. JARO 11(3):367–381

FUKUSHIMA K, FUKUSHIMA J, CHIN S ET AL (1996) Cross axis vestibulo-ocular reflex induced by pursuit training in alert monkeys. Neurosci Res 25:255–265

FURMAN JM, WALL C, KAMERER DB (1989) Earth horizontal axis rotational responses in patients with unilateral peripheral vestibular deficits. Ann Otol Rhinol Laryngol 98(7 Pt 1):551–555

GILLESPIE MB, MINOR LB (1999) Prognosis in bilateral vestibular hypofunction. Laryngoscope 109:35–41

GONG W, HABURCAKOVA C, MERFELD DM (2008) Vestibulo-ocular responses evoked via bilateral electrical stimulation of the lateral semicircular canals. IEEE Trans Biomed Eng 55(11):2608–2619

GRUNBAUER WM, DIETERICH M, BRANDT T (1998) Bilateral vestibular failure impairs visual motion perception even with the head still. NeuroReport 9(8):1807–1810

HARRISON REW, BAKER JF, ISU N, WICKLAND CR, PETERSON BW (1986) Dynamics of adaptive change in vestibulo-ocular reflex direction. I. Rotations in the horizontal plane. Brain Res 371:162–165

HASLWANTER T (1995) Mathematics of three-dimensional eye rotations. Vis Res 35:1727–1739

HAYDEN R, SAWYER S, FREY E, MORI S, MIGLIACCIO AA, DELLA SANTINA CC (2011) Virtual labyrinth model of vestibular afferent excitation via implanted electrodes: validation and application to design of a multichannel vestibular prosthesis. Exp Brain Res 210(3–4):623–640

HEPP K (1990) On listing's law. Commun Math Phys 132:285–295

HIRVONEN TP, MINOR LB, HULLAR TE, CAREY JP (2005) Effects of intratympanic gentamicin on vestibular afferents and hair cells in the chinchilla. J Neurophysiol 93(2):643–655

LASKER DM, HULLAR TE, MINOR LB (2000) Horizontal vestibuloocular reflex evoked by high-acceleration rotations in the squirrel monkey. III. Responses after labyrinthectomy. J Neurophysiol 83:2482–2496

LEWIS RF, GONG WS, RAMSEY M, MINOR L, BOYLE R, MERFELD DM (2002) Vestibular adaptation studied with a prosthetic semicircular canal. J Vestib Res 12:87–94

LEWIS RF, HABURCAKOVA C, GONG W, MAKARY C, MERFELD DM (2010) Vestibuloocular reflex adaptation investigated with chronic motion-modulated electrical stimulation of semicircular canal afferents. J Neurophysiol 103(2):1066–1079

MIGLIACCIO AA, SCHUBERT MC, JIRADEJVONG P, LASKER DM, CLENDANIEL RA, MINOR LB (2004) The three-dimensional vestibulo-ocular reflex evoked by high-acceleration rotations in the squirrel monkey. Exp Brain Res 159(4):433–446

MINOR LB (1998) Gentamicin-induced bilateral vestibular hypofunction. JAMA 279:541–544

MINOR LB, LASKER DM (2009) Tonic and phasic contributions to the pathways mediating compensation and adaptation of the vestibulo-ocular reflex. J Vestib Res 19(5–6):159–170

REMMEL RS (1984) An inexpensive eye movement monitor using the scleral search coil technique. IEEE Trans Biomed Eng 31(4):388–390

Robinson DA (1963) A method of measuring eye movement using a sclera search coil in a magnetic field. IEEE Trans Biomed Eng 10:137–145

Sadeghi SG, Minor LB, Cullen KE (2007) Response of vestibular-nerve afferents to active and passive rotations under normal conditions and after unilateral labyrinthectomy. J Neurophysiol 97(2):1503–1514

Sadeghi S, Minor LB, Cullen KE (2010) Neural correlates of motor learning: dynamic regulation of multimodal integration in the macaque vestibular system. J Neurosci 30(30):10158–10168

Schultheis LW, Robinson DA (1981) Directional plasticity of the vestibulo-ocular reflex in the cat. Ann NY Acad Sci 374:504–512

Straumann D, Zee DS, Solomon D, Lasker AG, Roberts DC (1995) Transient torsion during and after saccades. Vis Res 35:3321–3334

Tweed D, Cadera W, Vilis T (1990) Computing three-dimensional eye position quaternions and eye velocity from search coil signals. Vis Res 30(1):97–110

Ushio M, Minor LB, Della Santina CC, Lasker DM (2011) Unidirectional rotations produce asymmetric changes in horizontal VOR gain before and after unilateral labyrinthectomy in macaques. Exp Brain Res 210(3–4):651–660